

# Residual Stress Evaluation in L-PBF-Produced SS 316L Specimens

Matúš Geľatko , Michal Hatala , František Botko \*  and Radoslav Vandžura 

Faculty of Manufacturing Technologies, Technical University of Košice with a Seat in Prešov, 080 01 Prešov, Slovakia; matus.gelatko@tuke.sk (M.G.)

\* Correspondence: frantisek.botko@tuke.sk

**Abstract:** The identification of residual stresses (RS) in components made by selective laser melting (SLM) is necessary for subsequent technological optimization. The presented research is devoted to evaluating the influence of the combination of laser power ( $P$ ), scanning velocity ( $v$ ) and the rarely considered number of layers ( $n_L$ ) on surface residual stresses in SLM stainless steel SS 316L. Experimental parameters were set based on the Design of Experiment (DoE) method, with follow-up X-ray diffraction (XRD) measurements and data processing using analysis of variance (ANOVA) and regression analysis. The obtained data are a valuable stepping-stone for the subsequent design of research focused on the application of sustainable eco-friendly Abrasive Water Jet (AWJ) peening for RS modification in the evaluated material.

**Keywords:** additive manufacturing; selective laser melting; non-destructive testing; X-ray diffraction; stainless steel

## 1. Introduction

The surface integrity of materials is an important discipline that expresses their state from a qualitative point of view, including certain parameters that define its level. Stress is one of the most influential elements that participates at different phases of all manufacturing processes. The character and quantity of stress varies during individual operations and remains in the final component on non-zero values as residual stresses that can be compressive, which are normally positive, and tensile, which are normally considered to be negative, mainly due to their supportive character on the growth of discontinuities. Three main actuating mechanisms are the thermal phase transformation mechanism, thermal-plastic deformation mechanism and mechanical deformation mechanism. The first is commonly represented by sharp thermal gradients that cause material volume variations, e.g., during heat treatment. The second is commonly represented by the combination of mechanical and thermal load, which occurs during some machining technologies. The third is represented by the dominating mechanical load during technologies such as polishing or shot peening [1,2].

The SLM process is characterized by the input material in the form of powder, which is transformed into the solid state using the laser beam with high power impact. The powder becomes fully molten, is subsequently cooled and the final component is created by the layer-by-layer repetition of this operation. Considering that the material is subjected to the laser impact, which focuses its high energy on the one small point during the SLM process, actuating mechanisms of residual stress induction can be predicted in the form of sharp thermal gradients around this point. The material is not able to absorb this heat, the expanding surface layer is restricted by subsurface layers and compressive residual stresses arise. After reaching the yield strength of the material, plastic deformation of the surface layer occurs, which consequently leads to its shrinking during cooling, whereas this phenomenon is again restricted by subsurface layers; hence, the final residual stresses in the surface layer are of tensile character. Applying other surface layers causes the reduction of tensile stresses in the subsurface layers. In the final SLM component, maximal tensile



**Citation:** Geľatko, M.; Hatala, M.; Botko, F.; Vandžura, R. Residual Stress Evaluation in L-PBF-Produced SS 316L Specimens. *Materials* **2024**, *17*, 2270. <https://doi.org/10.3390/ma17102270>

Academic Editors: Guang Xu and Man Liu

Received: 21 April 2024

Revised: 7 May 2024

Accepted: 9 May 2024

Published: 11 May 2024



**Copyright:** © 2024 by the authors. Licensee MDPI, Basel, Switzerland. This article is an open access article distributed under the terms and conditions of the Creative Commons Attribution (CC BY) license (<https://creativecommons.org/licenses/by/4.0/>).

residual stresses are present on the surface with a decrease of their value deeper into the volume [3–5]. A variation in the stress state is influenced by factors included in Table 1.

**Table 1.** Factors influencing residual stresses in SLM components.

Tensile Residual Stresses	Factor
Increasing	Number of layers [3]
	Material yield strength [3]
	Overall energy input [5,6]
	Laser power [7,8]
	Scanning length [5]
Decreasing	Substrate thickness [3]
	Scanning velocity [5,7]
	Layer thickness [9]
	Scanning strategy [10,11]
	Re-scanning [12]
	Substrate preheating [11,12]

It is evident that several factors influence the induction of residual stresses during AM, but the key is the energy density that causes the variation in residual stresses, which is described within the experiment focused on the AM material AISI 316L [6]. Chiefly, the laser power and scanning velocity are the most crucial at this energy density. As was stated in one study [7], the most important factor can be defined as the main mechanism of energy input and the second most important can be defined as the main mechanism of cooling rate. A more significant induction of residual stresses occurs with increasing laser power, which can be considered a negative factor [8]. In contrast, the second factor can be considered the positive effect, due to the shorter duration of laser energy impact on the influenced area of the material with increasing of scanning velocity [5]. Authors Mercelis and Kruth [3] described the increasing residual stresses caused by the greater number of applied layers.

Considering the previously mentioned influence of residual stresses in the surface layers of the materials, X-ray diffraction non-destructive testing seems to be adequate for their measurement [13]. This was confirmed by recent studies focused on RS evaluation, where X-ray diffraction was applied to a wide portfolio of SLM materials. On the Al-12 Si aluminum alloy, XRD was used to record differences in residual stresses after the heat treatment at 540 °C for 1, 7 and 26 h [14]. Titanium alloy Ti6Al4V was the material of interest in the comprehensive study of the effect of selected post-processing technologies on basic material properties, where XRD took part in the evaluation of residual stresses [15]. During the monitoring of RS formation in Inconel 625 alloy, synchrotron XRD was used for the in situ measurement with promising results [16]. The effect of build location during the L-PBF technology on roughness and residual stresses (using XRD) in Maraging 300 steel was evaluated during the experiment performed by de Oliveira and co-authors [17]. Specimens of SLM 316L stainless steel were measured using X-ray diffraction during the experimental validation process of FEM analysis focused on the thermal and residual stress profile in identical material [18]. Chao et al. used the XRD method as a tool to monitor the influence of post-processing heat treatment (400–1400 °C) on residual stress relief and other properties of SLM 316L material [19]. Preheating and re-scanning techniques can similarly influence the behavior of residual stresses in SLM stainless steel, which was investigated using FEM analysis with XRD validation [12].

The design of experiment (DoE) method allows the statistical analysis of the effect of various technological parameters on monitored output parameters, not excluding residual stresses, such as those carried out within the experiment focused on GTAW (Gas Tungsten Arc Welding) [20], or the optimization of the SLM process parameters' influence on final porosity, experimentally conducted on AZ31 magnesium powder [21]. Such statistically oriented studies include the follow-up application of ANOVA (analysis of variance) [22] and regression analysis [23] for the expression of evaluated dependencies. Considering that

various analytical methods are crucial within the evaluation of processes [24], a combination of previously mentioned statistical methods with XRD non-destructive testing could be an appropriate tool for the prediction of induced surface residual stresses in SLM stainless steel based on the magnitude of selected technological parameters.

The presented experiment is focused on the evaluation of selected SLM parameters, considering the final surface residual stresses in SLM stainless steel with the application of methods, mentioned in the previous paragraph. The motivation for the research was to monitor the influence of selected parameters' combinations on final surface residual stresses, mainly due to the absence of experimental data related to the number of layers' influence and follow-up SLM process optimization. Various RS values in experimental specimens, obtained by the application of the DoE method, will be crucial for the subsequent setting of AWJ peening application, within research focused on their reduction.

## 2. Materials and Methods

The research was conducted using a Design of Experiment (DoE) method within the Minitab v21 statistical software, which allows the monitoring of the output data based on the input data, with the expression of their mutual relations and significance, whereas the output data (responses:  $y_1, y_2 \dots y_n$ ) are dependent on the input data (predictors:  $x_1, x_2 \dots x_m$ ), which are expressed by values defined as factorial levels. The number of runs for a certain number of predictors (factors) and their levels can be expressed by Equation (1) [25]:

$$n = \lambda^k \quad (1)$$

where  $\lambda$  represents the number of factorial levels (inputs) and  $k$  represents the number of factors. The primary objective is a definition of a mathematical model, expressing previously mentioned relations and the secondary objective is their subsequent analysis and graphical and numerical interpretation. The mathematical model, important for the optimization and subsequent experiments, can be expressed by a polynomial function, which corresponds to Equation (2) [25]:

$$y_i = b_0 + b_1 \times x_1 + b_2 \times x_2 + b_3 \times x_3 + b_{12} \times x_1 \times x_2 + b_{13} \times x_1 \times x_3 + b_{23} \times x_2 \times x_3 + b_{123} \times x_1 \times x_2 \times x_3 \quad (2)$$

where  $y_i$  is the observed value of output quantity  $y$  (response),  $x_{i1} \dots x_{ik}$  are values of input quantities (factors),  $b_0$  is the average value (intercept), and  $b_1 \dots b_{ik}$  are coefficients of regression equation [25]. For the experiment, three factors were selected in the form of laser power ( $P$ ), scanning velocity ( $v$ ) and number of layers ( $n_L$ ). For the response, resulting residual stresses  $\sigma$  were monitored on the surface layer of experimental specimens. The influence of the mentioned factors was analyzed at two levels with two replicates, which corresponds to the two-level factorial design of experiment  $2^3$  with an overall number of 16 repetitions. Therefore, 16 experimental specimens were made of SS 316L stainless steel (Tables 2 and 3) using the SLM technology, during which the powder material is made fully molten by the laser energy impact, and after its cooling, a homogenous structure is created. Specimens were prepared at the Technical University in Ostrava (Czech Republic) Protolab Center for 3D printing on a RenAM500S Flex machine by Renishaw company (Wotton-under-Edge, UK).

**Table 2.** Chemical composition of SS 316L stainless steel [26].

Element	Fe	Cr	Ni	Mo	Mn	Si	N	O	P	C	S
Mass (%)	Balance	16–18	10–14	2–3	≤2	≤1	≤0.1	≤0.1	≤0.045	≤0.03	≤0.03

Table 4 includes technological parameters of the experimental specimens' creation. Boundary values of parameters ( $P$ ,  $v$  and  $n_L$ ), representing factors within the two-level model, were set based on their influence on the porosity formation, which was monitored

within the recent research [27]. The reason was the evaluation of residual stresses in possibly the most homogenous material.

**Table 3.** Physical properties of SS 316L stainless steel [26].

Parameter	Value	Unit
Density (wrought)	7.99	$\text{g}\cdot\text{cm}^3$
Thermal conductivity	16.2	$\text{W}/\text{mK}$
Melting range	1371–1399	$^{\circ}\text{C}$
Coefficient of thermal expansion	$16\cdot 10^{-6}$	$\text{K}^{-1}$
Particle-size distribution	15–45	$\mu\text{m}$

**Table 4.** SLM process parameters.

Parameter	Symbol	Value	Unit
Laser power	P	200–300	W
Scanning velocity	v	500–800	$\text{mm}\cdot\text{s}^{-1}$
Hatching distance	d	110	$\mu\text{m}$
Layer thickness	$t_L$	50	$\mu\text{m}$
Number of layers	$n_L$	200–400	-
Scanning strategy		Meander (Figure 1)	
Gas protection		Argon (Ar)	

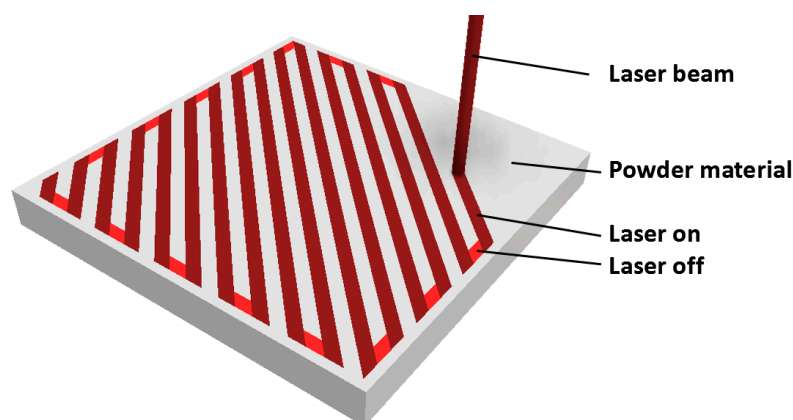


**Figure 1.** Meander scanning strategy used for SLM preparation of experimental specimens [28].

Specimens of cut square (Figure 2) were designed and prepared in dimensions  $30 \times 30$  mm and heights of 10 and 20 mm, based on the number of applied layers (200 and 400). A larger size of experimental specimens was selected with consideration to the conduction of subsequent experiments, focused on the application of Abrasive Water Jet (AWJ) peening. Table 5 includes values of selected SLM parameters for each specimen.

The X-ray diffraction (XRD) method was used for the evaluation of residual stresses in the surface layer of experimental specimens. Measurements were performed at the Department of Machining and Manufacturing Technologies at the University of Žilina on Proto iXRD machine with an MG40 goniometer by Proto company (Wrocław, Poland), using the parameters summarized in Table 6. Overall, 80 measurements were performed on 16 specimens.

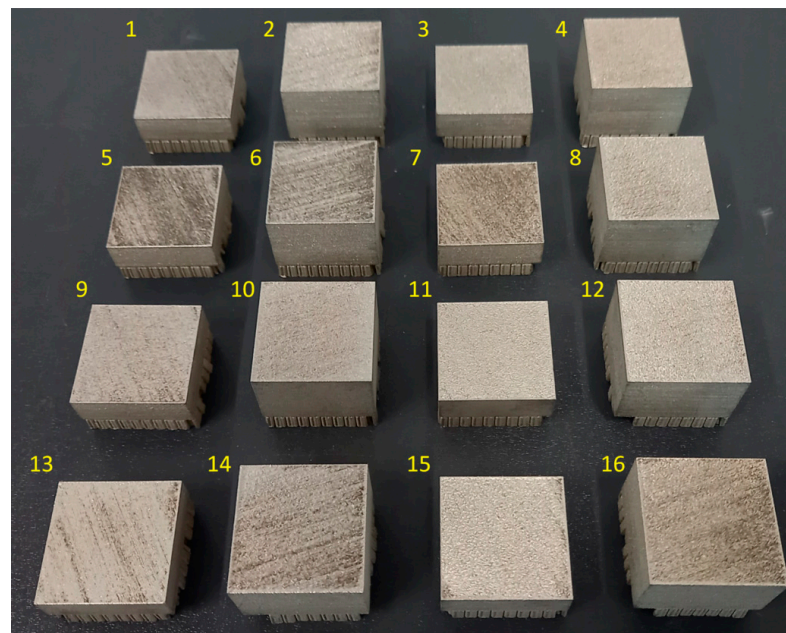


**Figure 2.** Experimental specimens made of SLM SS 316L material (according to DoE).

**Table 5.** Combinations of technological parameters within specimens.

Specimen	P [W]	v [mm·s <sup>-1</sup> ]	n <sub>L</sub> [mm]
1	200	500	200
2	200	500	400
3	200	800	200
4	200	800	400
5	300	500	200
6	300	500	400
7	300	800	200
8	300	800	400
9	200	500	200
10	200	500	400
11	200	800	200
12	200	800	400
13	300	500	200
14	300	500	400
15	300	800	200
16	300	800	400

**Table 6.** X-ray diffraction parameters.

Parameter	Value	Unit
X-ray tube	Mn_K ( $\alpha$ )	-
Filter	Cr	-
Collimator diameter	1	mm
Voltage	20	kV
Current	4	mA
Beta oscillation ( $\beta$ )	3	°
Number of angle positions	15 ( $\pm 30^\circ$ )	-
Penetration depth	10	$\mu\text{m}$
Number of points on specimen	5 (Figure 3)	-

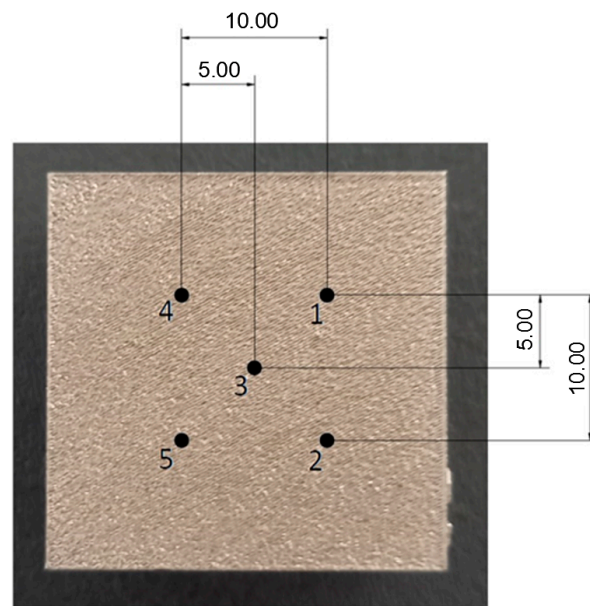


**Figure 3.** XRD measurement points on a surface layer of each specimen (dimensions in mm).

### 3. Results

Obtained values of normal surface residual stresses at five points on each specimen were averaged and these mean values were used as fundamentals for the subsequent evaluation of influencing factors in the form of selected technological parameters (Table 5).

As could be assumed, the residual stresses in the surface layers of all specimens, measured at all points, were of tensile character, which is characteristic for the residual stress induction mechanism caused by the impact of a laser beam with high energy density during SLM. The next diagram (Figure 4) allows the interpretation of values of residual stresses in individual points of specimens with included variances, representing a distribution uniformity of residual stresses in measured points, whereas a lower value indicates a higher uniformity. The lowest value of mean residual stresses was reached in the case of specimen 11 (60.28 MPa), which can be ascribed mainly to the influence of a higher scanning velocity  $v$  ( $800 \text{ mm}\cdot\text{s}^{-1}$ ) in combination with a lower laser beam power  $P$  (200 W). In contrast, the residual stresses with the highest mean value were present in specimen 6 at 395.1 MPa. The primary factor of such an elevated value can be predicted mainly as the influence of number of layers  $n_L$  (400) and scanning velocity  $v$  on the value of  $500 \text{ mm}\cdot\text{s}^{-1}$ .

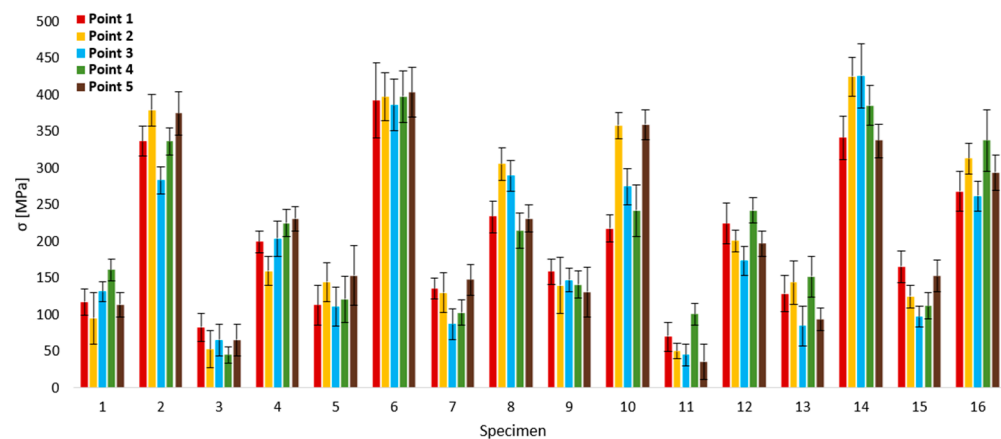


**Figure 4.** Residual stresses in individual points of specimens (XRD observed).

The lowest value of variance was reached at point 2 within the measurement of specimen 11, on the level 10.9 MPa. Inversely, the highest variance was reached at point 1 of specimen 6, with the value 51.2 MPa. Considering all measurements of residual stresses, the lowest value was in point 5 of specimen 11, equal to 35.9 MPa, and vice versa, the highest value of residual stress was present at point 3 of specimen 14, on level 425.6 MPa. A difference between the minimal and maximal values of residual stresses within individual specimens can be considered the indicator of their distribution in the area of five measurement points. Similarly to the variance, the lower the value, the more uniform the residual stress in the area of five measurement points. The mentioned difference was calculated with the lowest value within specimen 6 and with the highest value within specimen 10, equal to 17.5 MPa and 141.8 MPa, respectively.

To check the correctness of setting the limit values of the SLM parameters and their influence on the homogeneity of the microstructure, SEM analysis was performed on the surface layer of specimens within one replication (specimens 1–8). The evaluated specimens are composed of an austenitic microstructure, characteristic of low-carbon stainless steels. In comparison with conventional AISI 316L stainless steel, where the grains are equiaxed, the SLM process caused the creation of a typical LPB-F microstructure in the form of grains of irregular shapes and orientations. Certain grains tend to elongate in the direction of the path of the laser beam within the meander scanning strategy, which is depicted in a diagonal direction on the surface of specimen 1 in Figure 5.

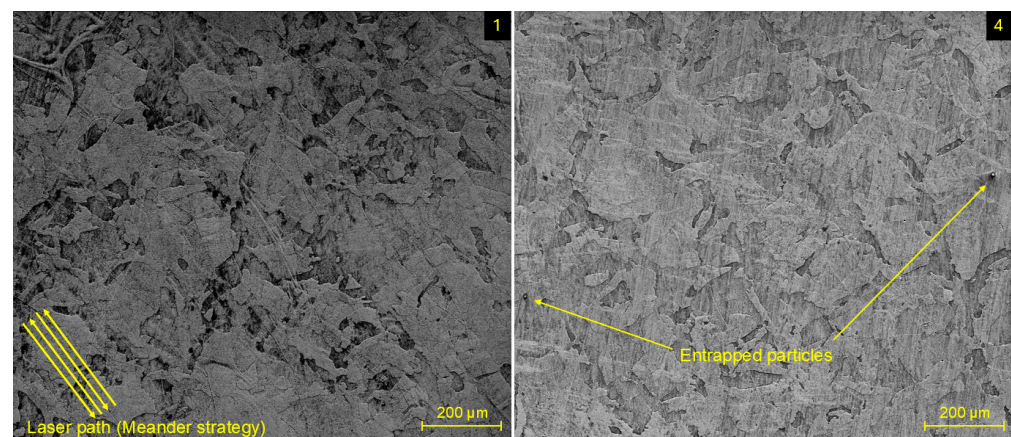


**Figure 5.** Microstructure of experimental specimens 1 and 4.

SEM image of specimen 4 (Figure 5) revealed the presence of powder particles entrapped within its microstructure. Such irregularities are common during all kinds of L-PBF processes, where sporadic insufficient melting of individual particles can occur. The presence of such single particles was observed in a negligible number within all evaluated specimens. In addition to the entrapped particle, Figure 6 depicts the occurrence of porosity in a microstructure of specimen 2 and specimen 8. Such types of voids, as the consequence of gas entrapment in the local melt pool during the cooling process, were not recorded in a systematic order and similarly were present in a negligible number.

At a higher magnification, inclusions on the grain interfaces were recorded for all evaluated specimens (Figure 7). Such discontinuities were present in the form of clusters containing the set of smaller inclusions and also in the form of individual inclusions of bigger size. A potential explanation for their presence can be a  $\delta$ -ferrite, as the consequence of the precipitation process at numerous preheating temperatures, which take place during the SLM process when a heat source influences the material multiple times throughout the transition of a laser beam. The elevated percentage of Cr and Mo elements in material composition supports the creation of this phase, due to their ferrite-forming nature [29].

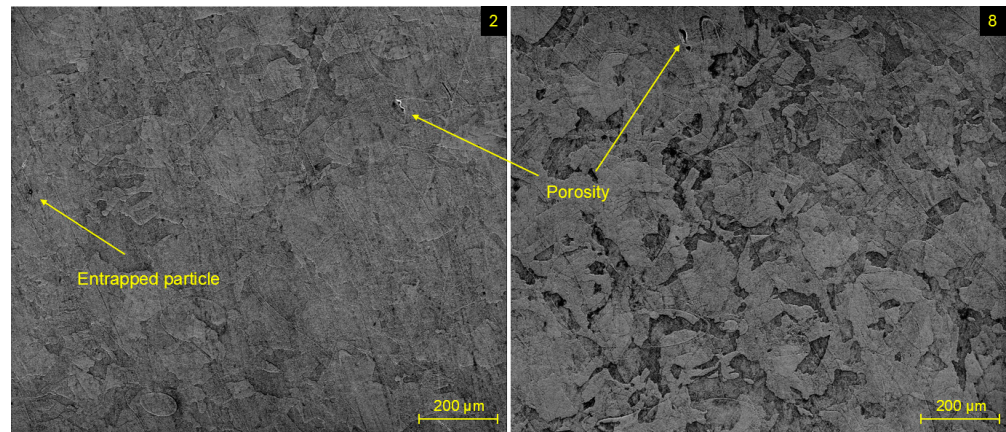


**Figure 6.** Microstructure of experimental specimens 2 and 8 with entrapped particles and porosity.

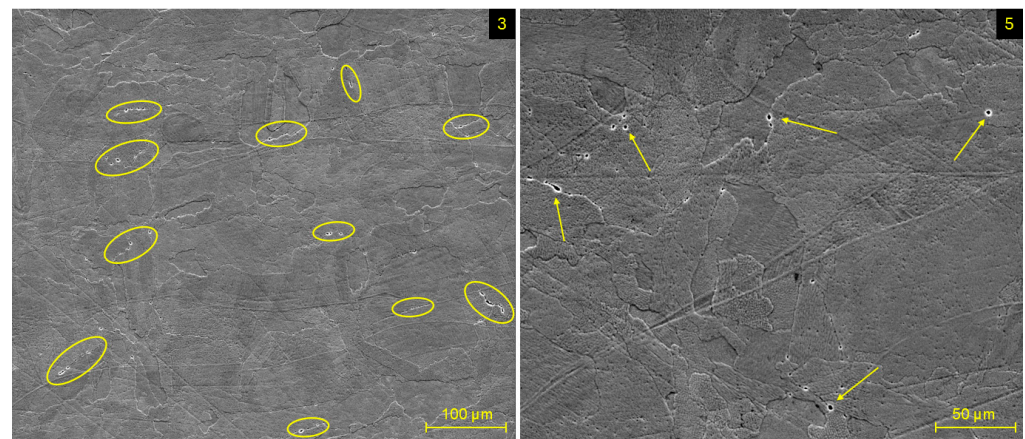


**Figure 7.** Inclusion on grain boundaries in specimens 3 and 5.

Figure 8 includes an SEM image of the microstructure at the level of the grains, and a size of 10–50  $\mu\text{m}$  was observed for all experimental specimens. These austenitic grains are composed of a fine cellular structure, which arises during the SLM process, mainly as a consequence of the rapid cooling of molten material. The cellular structure is variously oriented within grains, whereas its reorientation during the change of morphology arises without some external mechanism in the areas of grain boundaries, scan trace boundaries, or melt pool interfaces. Also, previously described inclusions on grain boundaries were observed in Figure 8.

It can be stated that the SEM observed data confirmed the correctness of setting the limit values of SLM parameters, considering the integrity of the microstructure. Observed discontinuities in selected specimens were shown to be obvious for the manufacturing process used for the material (SLM)—sporadic entrapped powder particles and precipitation inclusions on grain boundaries, or voids in the form of gas-entrapment porosity that were identified randomly, in negligible number and smaller sizes. The influence of such discontinuities on the RS character, their magnitude and other mechanical properties can be considered insignificant; thus, the RS can be evaluated only with respect to the SLM parameters.

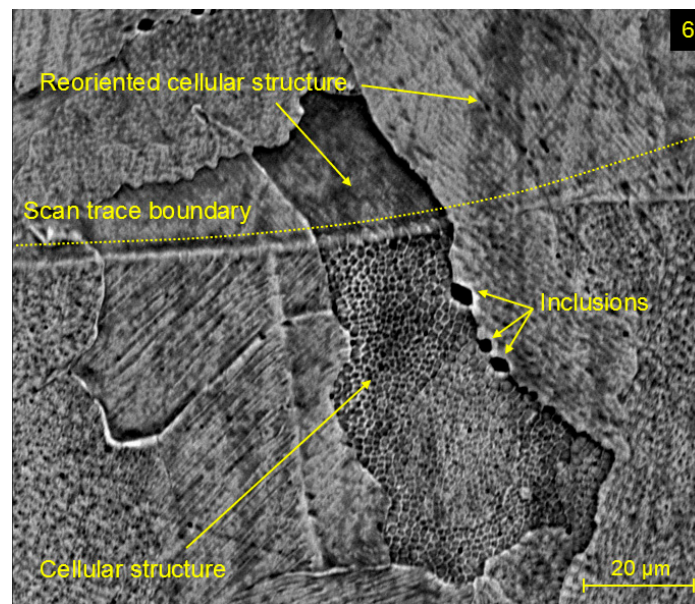


**Figure 8.** SEM image of grain interface in the microstructure of experimental specimen 6.

### 3.1. Analysis of Variance (ANOVA)

The mean values of residual stresses were used for the creation of analysis of residual stresses on the surface layer of the experimental material. The selected factors ( $P$ ,  $v$  and  $n_L$ ) were evaluated in terms of their influence on the residual stress response ( $\sigma$ ), using the analysis of variance method (ANOVA), based on which their statistical significance can be assessed, where the key parameter is the  $p$ -value (Table 7). For the assessment of statistical significance, the  $p$ -value is considered with respect to the level of significance  $\alpha = 0.05$ . Considering that the mentioned value did not exceed this level at any factor, the null hypothesis  $H_0$  can be accepted and, consequently, the individual factors were regarded as statistically significant. The calculated coefficient of determination  $R^2$  is 0.9610, which means that the model can be applied in 96.10% of similar cases, as described by Equation (3). The statistical significance of the described model is also confirmed by the adjusted coefficient of determination  $R^2_{Adj}$  with a value of 0.9468 at the 94.68% level.

**Table 7.** Analysis of variance (ANOVA) for residual stresses.

Source	DF	Adj SS	Adj MS	F-Value	$p$ -Value
Regression	4	174,885	43,721	67.74	0.000
Linear	3	168,986	56,329	87.27	0.000
$P$	1	9707	9707	15.04	0.003
$v$	1	21,938	21,938	33.99	0.000
$n_L$	1	137,341	137,341	212.78	0.000
2-Way Interactions	1	5899	5899	9.14	0.012
$v \cdot n_L$	1	5899	5899	9.14	0.012
Error	11	7100	645		
Lack-of-Fit	3	4597	1532	4.90	0.032
Pure Error	8	2503	313		
Total	15	181,985			

### 3.2. Regression Analysis

As previously mentioned, Equation (3) expresses the residual stresses ( $\sigma$ ) induced in the surface layer of the experimental material, as the response to the influence of selected factors in the form of laser power ( $P$ ), scanning velocity ( $v$ ) and number of layers ( $n_L$ ).

$$\sigma = -286.6 + 0.493 \times P + 0.137 \times v + 175.9 \times n_L - 0.001280 \times v \times n_L \quad (3)$$

The Pareto chart of the standardized effects (Figure 9) shows an interpretation of the result of individual factors' significance analysis in the form of technological parameters, including their combinations for the subsequent creation of a regression model. The most influential factor with a significantly higher value was shown to be factor C, which corresponds to the number of layers  $n_L$  on the value 14.6. The second most significant influence had factor B, which represents the scanning velocity  $v$  and the factor with the least significance was factor A, representing the power of laser beam  $P$ , on the values 5.83 and 3.88, respectively. In addition to the mentioned three individual factors, the BC factor corresponding to the combination of scanning velocity  $v$  and a number of layers  $n_L$  (3.02) is present above the limit of the critical value of standardized effect (2.20). All these factors are important for the creation of a regression model. Reversibly, other 2 and 3-factorial combinations (AC—1.72, AB—1.51, ABC—1.37) are below the limit of critical value; hence, they are negligible for the creation of a regression model.

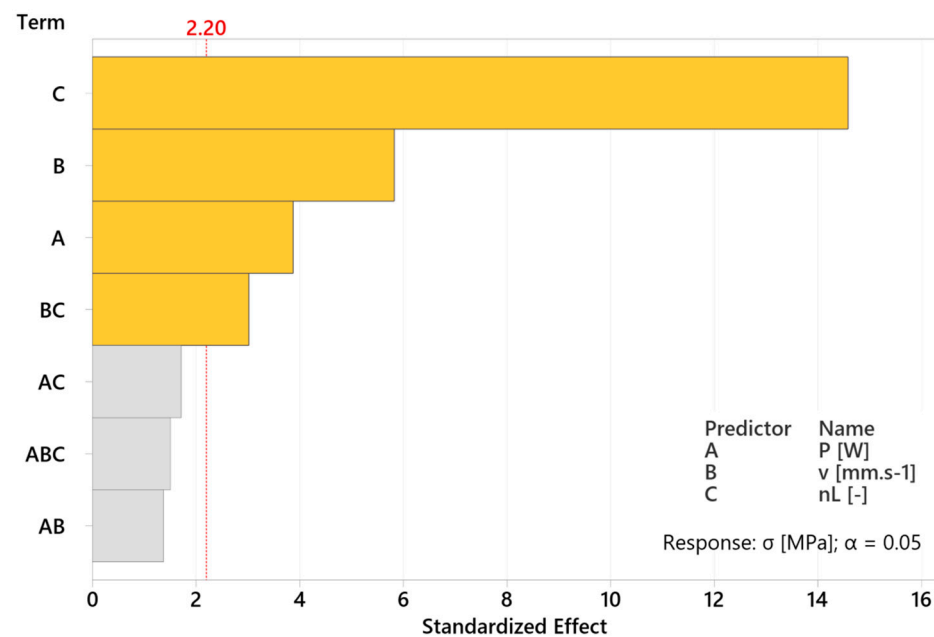


Figure 9. Pareto chart of standardized effects ( $P$ ,  $v$ ,  $n_L$  and their interactions) on RS.

A normal probability plot of residual distribution, within a described regression model, is shown in Figure 10. It can be stated that the distribution of residuals acquires a state of normality, taking the positions of individual points, which are situated in the close area of the curve, representing the ideal state, with minimal deviations. Any of included points did not exceed value 2 of the Standardized Residual and most of them are present in the range of the Standardized Residual value 1 in both directions, which confirms the correctness of the regression model.

The main effects plot, included in Figure 11, puts selected individual factors ( $P$ ,  $v$  and  $n_L$ ) and values of residual stresses ( $\sigma$ ) into proportion, by which the influence of independent variables on a dependent variable within the regression model are interpreted. The reference line is on 203.7 MPa. It is evident that the least significant influence on the induction of residual stresses is present in the given range of laser power  $P$  values. However, this parameter needs to be taken into account, due to the increase in induced residual stresses with its increase, which can be considered a negative influence. The magnitude of residual stresses varies from 179.1 MPa at 200 W to a maximum of 228.3 MPa at 300 W. The scanning velocity ( $v$ ) influences the formation of residual stresses in a greater manner, but it needs to be pointed out that this influence is positive, because the residual stress value decreases with increases in velocity, due to the shorter time of laser power impact into the single point. The maximum was reached at 500 mm.s<sup>-1</sup> at 240.7 MPa and

decreased to 166.7 MPa at  $800 \text{ mm.s}^{-1}$ . The most significant influence was recorded at the number of layers ( $n_L$ ), when a radical graduation of tensile residual stress component occurs with the increasing of layers. The overall maximum of all factors was reached at 296.3 MPa at 400 layers to the smallest value 111 MPa at 200 layers.

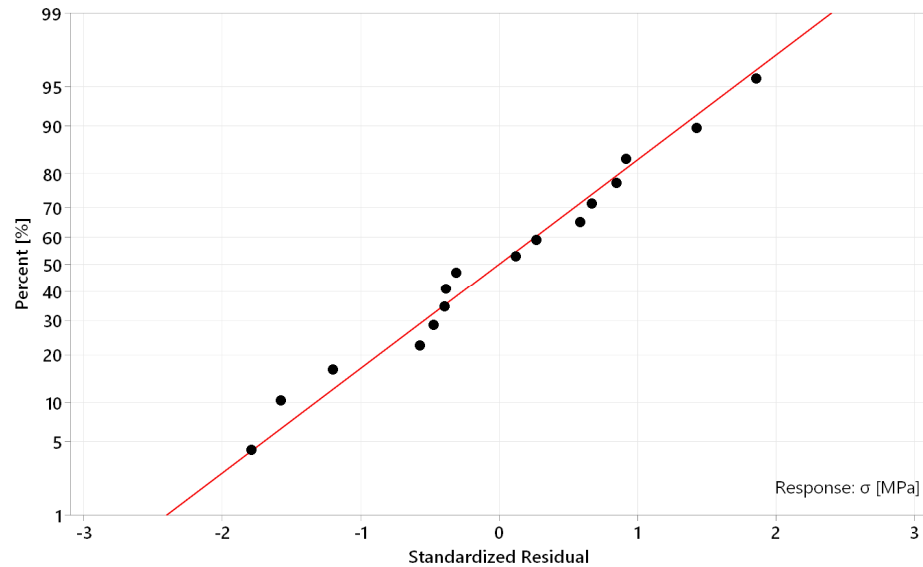


Figure 10. Normal probability plot of standardized residual distribution.

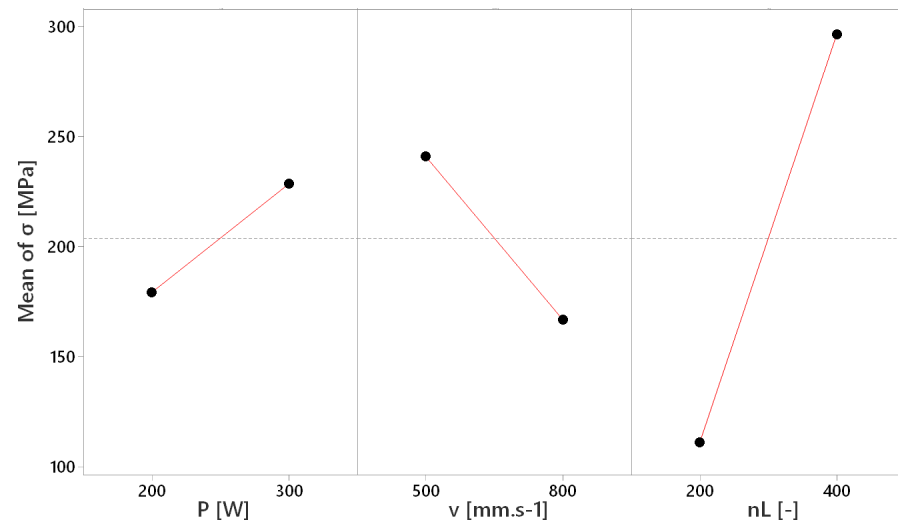
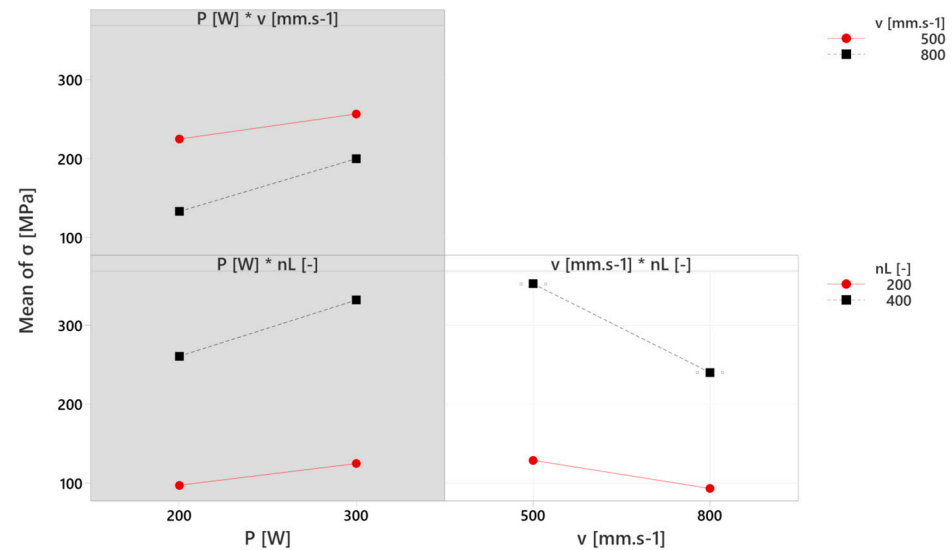


Figure 11. Plot of main effects ( $P$ ,  $v$  and  $n_L$ ) on residual stresses ( $\sigma$ ).

The interactions of individual factors and the influence of their combinations on the resulting residual stresses are included in Figure 12. The interaction plot for residual stresses  $\sigma$  [MPa] includes three partial graphs corresponding to each combination. The left upper graph includes the interaction of laser power ( $P$ ) with scanning velocity ( $v$ ) and it confirms, as previously described, the least influence of laser power on the increasing residual stresses, which can be restricted by increasing the scanning velocity (to  $800 \text{ mm.s}^{-1}$ ), where residual stresses can be decreased to 133.3 MPa. The lower graph on the left side includes the interaction of laser power ( $P$ ) and the number of layers ( $n_L$ ), where the negative effect of the laser power is in this case supported by the increasing of layers, which is confirmed by the black dashed curve on the higher values of stresses and with the steeper slope. These two described interactions on the left side with the grey background were considered less significant and were not included in the creation of the regression model. The interaction

of scanning velocity ( $v$ ) and the number of layers ( $n_L$ ) was included in the creation of the regression model (white background) and its significance is confirmed by the steeper slope of the obtained curves, reaching higher values of residual stresses mainly in the case of the 400 layers. However, the curves are oriented in the direction of positive effect, due to the decrease of residual stresses with increasing scanning velocity.



**Figure 12.** Interaction plot of factors ( $P$ ,  $v$  and  $n_L$ ) effect on residual stresses ( $\sigma$ ).

The following surface plots show the influence of two-factorial interactions (independent variables) on the response (dependent variable) in the form of residual stresses ( $\sigma$ ), when the third factor is set to the mean value. The first diagram (Figure 13) depicts the combined influence of laser power ( $P$ ) and scanning velocity ( $v$ ) at 300 layers ( $n_L$ ). It is evident that a higher value of factor  $P$  causes an increased response ( $\sigma$ ), which can be considered a negative influence. The maximum above 250 MPa was reached at 300 W and 500 mm.s<sup>-1</sup>. However, with the increase of factor  $v$ , which has a positive effect, a decrease of response ( $\sigma$ ) occurs to a minimum of approx. 150 MPa at 200 W and 800 mm.s<sup>-1</sup>. It can be stated that increasing factor  $v$  leads to a decrease in negative factor  $P$  within the specified regression model.

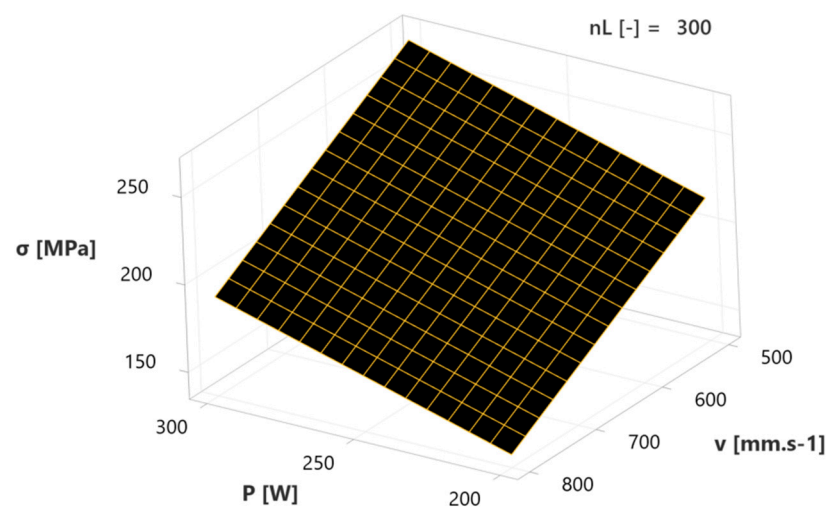


**Figure 13.** Surface plot of laser power—scanning velocity interaction influence on RS.

The next diagram (Figure 14) depicts a combination of the effect of laser power ( $P$ ) and number of layers ( $n_L$ ) at a mean value of scanning velocity ( $v = 650$  mm.s<sup>-1</sup>). The

maximum of residual stresses (approx. 300 MPa) is reached at a combination of 300 W with 400 layers and vice versa; the minimum value, approx. 100 MPa, is present at a combination of 200 W and 200 layers. Hence, the interaction of these two independent variables can be considered the negative effect of a specified regression model, due to the more significant induction of residual stresses ( $\sigma$ ), caused by the increasing dependent variables' values.

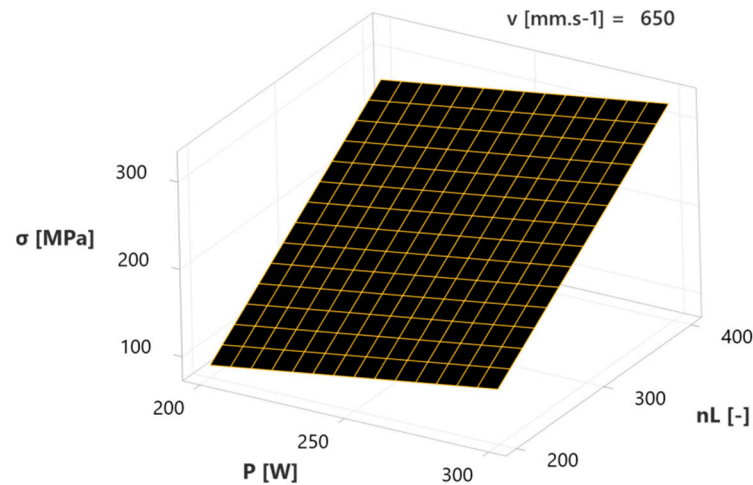


**Figure 14.** Surface plot of laser power—number of layers interaction influence on RS.

The third diagram (Figure 15) includes the effects of the interaction of factors  $v$  and  $n_L$  at the mean value (250 W) of the third factor  $P$ . Similar to in a previous diagram (Figure 14), a dependence confirms the most significant effect of number of layers ( $n_L$ ) within the specified regression model, whereas in this case its influence can be restricted by the increase in positive effect values, in the form of scanning velocity ( $v$ ), where at a combination of 200 layers and 800 mm.s<sup>-1</sup>, 100 MPa residual stresses are present. However, in the case of higher values of  $n_L$  (up to 400) and lower values of  $v$  (up to 500 mm.s<sup>-1</sup>), a considerable increase in response value ( $\sigma$ ) occurs, with its maximum at 300 MPa.

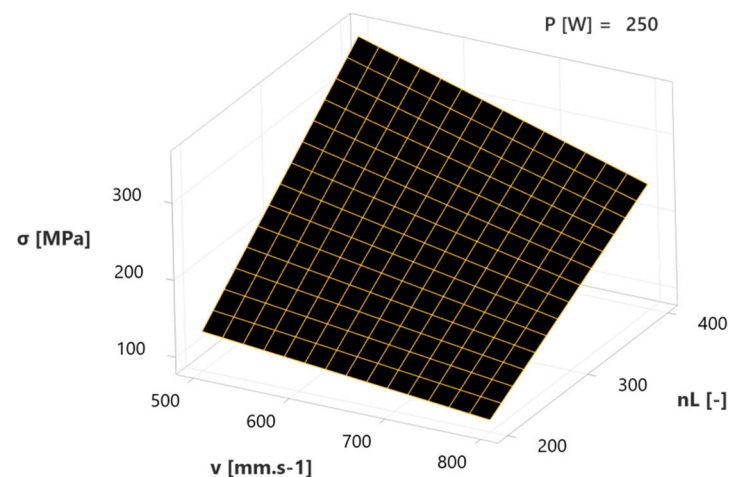


**Figure 15.** Surface plot of scanning velocity—number of layers interaction influence on RS.

#### 4. Discussion

The obtained results of the described experiment are similar to the results of other studies in the field. The increase in residual stresses was recorded under the influence of setting the higher values of laser power (160 and 200 W) at the fixed scanning velocity (600 mm.s<sup>-1</sup>) within one study [8], which was confirmed by the described results, where higher values of residual stresses were measured at a higher laser power (Figure 11). During another

experiment [6], the influence of overall energy density input was monitored, whereas its variability was reached by the various scanning velocities due to its more significant influence on residual stresses. It was confirmed within a study [5], where lower residual stresses were reached through increasing the scanning velocity (200, 400 and 800 mm.s<sup>-1</sup>) at a fixed laser power (200 W) and by the results interpreted in Figures 9 and 13. However, FEM analysis with the experimental verification made by Waqar, Guo and Sun [18] points to the opposite consequence of increasing the scanning velocity. Similar to the case of increasing the laser power, the induction of residual stresses of higher values occurred. An older study [3] describes the number of applied layers as a significant residual stress factor. The mentioned parameter was shown to be the most influential within the described experiment (Figures 9 and 11), and the only significant factorial interaction of the described regression model was reached by combining the number of layers with scanning velocity, whereas the first mentioned was more significant (Figure 15). Measured values of residual stresses within the experiment were similar to values stated within the referenced studies. Furthermore, we used a combination of statistical methods (DoE, ANOVA and regression analysis) provided the expression of individual and mutual dependencies of selected SLM parameters and their influence on RS in experimental stainless steel. A rarely considered factor in the form of the number of applied layers is shown to be important as individuals, so within interactions. Limits were set for the mentioned parameters in order to obtain a microstructure with the absence of significant voids (confirmed by SEM), which demonstrates the added value of the described experiment.

## 5. Conclusions

The described experiment includes results of the identification of residual stresses in a surface layer of SS 316L specimens made by SLM technology, measured using XRD. Specimens were manufactured using various combinations of technological parameters based on a DoE method, which subsequently served as input values for the statistical analysis of these factors on a residual stress state within the evaluated material. Based on experimental output data, the following conclusions can be derived:

- Promising application of Design of Experiments, ANOVA and regression analysis methods as suitable analytical tools for the evaluation of SLM technological parameters and their influence on final residual stresses in a surface layer of stainless steel.
- Proposal of regression equation based on the designed regression model, which could help to optimize the SLM process under similar conditions, considering the magnitude of induced residual stresses.
- The expression of correlations between selected technological parameters and induced residual stresses. A well-known negative effect of increasing laser power was confirmed and a considerably larger influence of a number of layers was presented. A positive effect of increasing scanning velocity was shown to be an effective tool for decreasing the negative effect of the other two factors.
- Effect on the residual stresses of mutual interactions between selected factors was described, with a significant influence of scanning velocity in combination with a number of layers.

Despite the promising obtained results, it is necessary to extend the presented research, which could help to optimize technology to a greater extent. Appropriate tools could include the application of more levels within individual factors (3-level model) and the use of center points. Increasing the replicates in the form of a higher number of experimental specimens could help to improve the credibility of the conducted regression analysis. A significant factor in the form of a number of applied layers seems to be obvious and necessary due to the dimensions of the final component. However, its influence and the influence of other factors are good to know, due to their prediction during the setting of appropriate parameters of post-processing operations.

**Author Contributions:** Conceptualization, M.G. and M.H.; methodology, M.G. and F.B.; software, R.V. and F.B.; validation, M.G.; formal analysis, R.V.; investigation, M.G.; resources, F.B. and R.V.; data curation, M.H. and F.B.; writing—original draft preparation, M.G. and R.V.; writing—review and editing, M.H. and F.B.; visualization, R.V.; supervision, M.H.; project administration, M.G. and F.B.; funding acquisition, M.H. All authors have read and agreed to the published version of the manuscript.

**Funding:** This work was funded by the Slovak Research and Development Agency under contract No. APVV-21-0228 and the projects VEGA 1/0391/22 and KEGA 017TUKE-4/2023 were granted by the Ministry of Education, Science, Research and Sport of the Slovak Republic. The article is the result of implementing the following project: Development of excellent research capacities in the field of additive technologies for the industry of the 21st century, ITMS: 313011BWN5, supported by the Operational Program Integrated Infrastructure funded by the ERDF.

**Institutional Review Board Statement:** Not applicable.

**Informed Consent Statement:** Not applicable.

**Data Availability Statement:** Data are contained within the article.

**Acknowledgments:** The authors would like to thank the Protolab Center for 3D Printing (VSB-TU Ostrava) for the preparation of experimental specimens and Department of Machining and Manufacturing Technologies (University of Žilina) for X-ray diffraction measurements.

**Conflicts of Interest:** The authors declare no conflicts of interest. The funders had no role in the design of the study; in the collection, analyses or interpretation of the data; in the writing of the manuscript; or in the decision to publish the results.

## References

1. Davim, J.P. (Ed.) *Surface Integrity in Machining*; Springer: London, UK, 2010. [\[CrossRef\]](#)
2. Withers, P.J.; Bhadeshia, H.K.D.H. Residual stress. Part 2—Nature and origins. *Mater. Sci. Technol.* **2001**, *17*, 366–375. [\[CrossRef\]](#)
3. Mercelis, P.; Kruth, J.P. Residual stresses in selective laser sintering and selective laser melting. *Rapid Prototyp. J.* **2006**, *12*, 254–265. [\[CrossRef\]](#)
4. Fang, Z.C.; Wu, Z.L.; Huang, C.G.; Wu, C.W. Review on residual stress in selective laser melting additive manufacturing of alloy parts. *Opt. Laser. Technol.* **2020**, *129*, 106283. [\[CrossRef\]](#)
5. Liu, Y.; Yang, Y.; Wang, D. A study on the residual stress during selective laser melting (SLM) of metallic powder. *Int. J. Adv. Manuf. Technol.* **2016**, *87*, 647–656. [\[CrossRef\]](#)
6. Simson, T.; Emmel, A.; Dwars, A.; Böhm, J. Residual stress measurements on AISI 316L samples manufactured by selective laser melting. *Addit. Manuf.* **2017**, *17*, 183–189. [\[CrossRef\]](#)
7. Wang, L.; Jiang, X.; Zhu, Y.; Zhu, X.; Sun, J.; Yan, B. An approach to predict the residual stress and distortion during the selective laser melting of AlSi10Mg parts. *Int. J. Adv. Manuf. Technol.* **2018**, *97*, 3535–3546. [\[CrossRef\]](#)
8. Bian, P.; Shi, J.; Liu, Y.; Xie, Y. Influence of laser power and scanning strategy on residual stress distribution in additively manufactured 316L steel. *Opt. Laser Technol.* **2020**, *132*, 106477. [\[CrossRef\]](#)
9. Mugwagwa, L.; Yadroitsev, I.; Matope, S. Effect of process parameters on residual stresses, distortions, and porosity in selective laser melting of maraging steel 300. *Metals* **2019**, *9*, 1042. [\[CrossRef\]](#)
10. Mugwagwa, L.; Dimitrov, D.; Matope, S.; Yadroitsev, I. Evaluation of the impact of scanning strategies on residual stresses in selective laser melting. *Int. J. Adv. Manuf. Tech.* **2019**, *102*, 2441–2450. [\[CrossRef\]](#)
11. Hajnys, J.; Pagáč, M.; Měsíček, J.; Petru, J.; Król, M. Influence of scanning strategy parameters on residual stress in the SLM process according to the bridge curvature method for AISI 316L stainless steel. *Materials* **2020**, *13*, 1659. [\[CrossRef\]](#)
12. Waqar, S.; Guo, K.; Sun, J. Evolution of residual stress behavior in selective laser melting (SLM) of 316L stainless steel through preheating and in-situ re-scanning techniques. *Opt. Laser Technol.* **2022**, *149*, 107806. [\[CrossRef\]](#)
13. Šafář, M.; Valíček, J.; Harničárová, M.; Šajgalík, M.; Tozan, H.; Kušnerová, M.; Drbúl, M.; Kadnár, M.; Czán, A. Proposal for the identification of residual stresses after turning and hardening of bearing steel. *Front. Mater.* **2023**, *10*, 1238816. [\[CrossRef\]](#)
14. Park, S.; Kim, S.H.; Park, J.; Lee, E. Al-12Si alloy fabricated via selective laser melting: Residual stress and microstructural factors after heat treatment. *J. Mater. Eng. Perform.* **2024**, *33*, 2156–2165. [\[CrossRef\]](#)
15. Önder, S.; Saklakoğlu, N.; Sever, A. Selective laser melting of Ti6Al4V alloy: Effect of post-processing on fatigue life, residual stress, microstructure, microhardness and surface roughness. *Mater. Charact.* **2023**, *196*, 112571. [\[CrossRef\]](#)
16. Schmeiser, F.; Krohmer, E.; Schell, N.; Uhlmann, E.; Reimers, W. Experimental observation of stress formation during selective laser melting using in situ X-ray diffraction. *Addit. Manuf.* **2020**, *32*, 101028. [\[CrossRef\]](#)
17. de Oliveira, A.R.; Santos, S.F.; Jardini, A.L.; Del Conte, E.G. Surface Residual Stress and Roughness Mapping for Different Build Locations in Laser Powder Bed Fusion of Maraging Steel. *J. Mater. Eng. Perform.* **2024**, *33*, 4065–4073. [\[CrossRef\]](#)

18. Waqar, S.; Guo, K.; Sun, J. FEM analysis of thermal and residual stress profile in selective laser melting of 316L stainless steel. *J. Manuf. Process.* **2021**, *66*, 81–100. [[CrossRef](#)]
19. Chao, Q.; Thomas, S.; Birbilis, N.; Cizek, P.; Hodgson, P.D.; Fabijanic, D. The effect of post-processing heat treatment on the microstructure, residual stress and mechanical properties of selective laser melted 316L stainless steel. *Mater. Sci. Eng. A-Struct.* **2021**, *821*, 141611. [[CrossRef](#)]
20. Baisukhan, A.; Nakkiew, W.; Pitjarnit, S. Design of experiment for predicting residual stresses in Gas Tungsten Arc Welding process. *Ind. Eng. Manag. Sci. Appl.* **2015**, *349*, 77–84. [[CrossRef](#)]
21. Pawlak, A.; Rosienkiewicz, M.; Chlebus, E. Design of experiments approach in AZ31 powder selective laser melting process optimization. *Arch. Civ. Mech. Eng.* **2017**, *17*, 9–18. [[CrossRef](#)]
22. Alzyod, H.; Ficzer, P. Material-dependent effect of common printing parameters on residual stress and warpage deformation in 3D printing: A comprehensive finite element analysis study. *Polymers* **2023**, *15*, 2893. [[CrossRef](#)] [[PubMed](#)]
23. Zhan, Y.; Liu, C.; Zhang, J.; Mo, G.; Liu, C. Measurement of residual stress in laser additive manufacturing TC4 titanium alloy with the laser ultrasonic technique. *Mater. Sci. Eng. A-Struct.* **2019**, *762*, 138093. [[CrossRef](#)]
24. Duhancik, M.; Krenicky, T.; Coranic, T. Design and Testing of a Measurement Device for High-Speed Bearing Evaluation. *Appl. Sci.* **2024**, *14*, 508. [[CrossRef](#)]
25. Miller, I. *DOE: Návrh a Analýza Experimentu s Pomocí MINITAB®*; Interquality: Prague, Czech Republic, 2010.
26. Data Sheet: SS 316L-0407 Powder for Additive Manufacturing. Available online: <https://www.renishaw.com/resourcecentre/en/details/data-sheet-ss-316l-0407-powder-for-additive-manufacturing--90802> (accessed on 11 April 2024).
27. Hajnyš, J. Výzkum Vlivu Dokončovacích Operací na Modifikaci Užitečných Vlastností Součástí Vyrobených Aditivní Technologií. Dissertation Thesis, VSB-Technical University of Ostrava, Ostrava, The Czech Republic, 2019.
28. Meander Tripe and Chessboard Hatching Pattern. Available online: <https://www.renishaw.com/resourcecentre/en/details/Meander-stripe-and-chessboard-hatchings-pattern--95492?lang=en> (accessed on 11 April 2024).
29. Morozova, I.; Kehm, C.; Obrosof, A.; Yang, Y.; Mohammad Miah, K.U.; Uludintceva, E.; Fritzsche, S.; Weiß, S.; Michailov, V. On the Heat Treatment of Selective-Laser-Melted 316L. *J. Mater. Eng. Perform.* **2023**, *32*, 4295–4305. [[CrossRef](#)]

**Disclaimer/Publisher’s Note:** The statements, opinions and data contained in all publications are solely those of the individual author(s) and contributor(s) and not of MDPI and/or the editor(s). MDPI and/or the editor(s) disclaim responsibility for any injury to people or property resulting from any ideas, methods, instructions or products referred to in the content.